

The dependence of transverse and longitudinal resolutions on incident Gaussian beam widths in the illumination part of optical scanning microscopy

Hyung-Su Chon, Giseung Park, Sang-Bum Lee, Seokchan Yoon, Jaisoon Kim,
Jai-Hyung Lee, and Kyungwon An

School of Physics, Seoul National University, Seoul 151-747, Korea

kwana@phya.snu.ac.kr

The intensity distribution of a Gaussian laser beam is analyzed theoretically and experimentally when it is focussed by an objective lens with its numerical-aperture up to 0.95. It is found that the resulting values of full width at half maximum (FWHM) at the focus in the x and z directions are not much different from the ultimate FWHM values when the initial beam waist is equal to the entrance pupil radius of the objective lens. In addition, the increase in FWHM values is less than 100% even when the initial waist is further reduced to a half. © 2019 Optical Society of America

OCIS codes: 110.0180, 350.5730, 050.1960

1. Introduction

The spatial resolution in optical scanning microscopy is critically dependent on the beam spot size near the focus of a scanning objective lens. In general, the intensity distribution near the focus can be calculated by the electromagnetic diffraction theory of Richards and Wolf and Wolf.^{1,3} This theory is based on the vectorial equivalent of the Kirchhoff-Fresnel integral^{4,5} in the Debye approximation.^{4,5} In many experiments using an objective lens we usually assume that the incident beam is a plane wave apertured by the entrance pupil of the objective lens. However, the light source in the optical scanning microscopy is often a Gaussian laser beam, not an ideal plane wave. One can expand the Gaussian beam and let the central part of it, simulating a plane wave, incident on the objective lens. A practical question is then how large the beam should be expanded with respect to the entrance pupil size of the objective lens in order to obtain a spatial resolution comparable to that with the ideal plane wave input. To answer this question, we need to know the near-focal plane

intensity distribution of a Gaussian laser beam with an initial beam width w_0 when focused by an objective lens with an entrance pupil diameter D .

The intensity distribution in the region of focus have been measured in several experiments by using a knife-edge^{6,7} and a tapered fiber.^{8,9} However, a systematic investigation of the near-focus intensity distribution in the non-paraxial regime as a function of the input Gaussian beam width w_0 has not been performed to our knowledge. In the present work, we varied the input beam width incident on objective lenses with a numerical aperture (NA) of 0.4, 0.75 and 0.95, respectively, and measured the transverse (xy profile) and longitudinal (yz profile) intensity distributions of the focused beam by scanning a pinhole of 0.5 μm diameter along or perpendicular to the optic axis of the objective lens. From the measured distribution we determined the transverse and longitudinal beam spot sizes associated with the illumination part of our scanning microscope.

We found that the incident beam waist w_0 (half width) need not be much larger than the entrance pupil radius R ($= D/2$) in order to achieve a resolution comparable to that obtainable with a plane wave input. Particularly, when $w_0 = R$, both xy and yz beam spot sizes differ by less than 5% from their ultimate beam spot sizes in our calculations and by at most 20% even in actual measurements, which are subject to lens aberrations. We also found that one can allow the initial beam waist to be as small as $R/2$ only to increase FWHM values by twice from the ultimate FWHM values.

This paper is organized as follows. In Sec. 2, we first theoretically examine transverse and longitudinal FWHM's near the focal plane for an arbitrary input beam waist w_0 and then derive approximations for limiting cases, $w_0 \ll R$ and $w_0 \gg R$. Experimental setup is described in Sec. 3 and results and discussion are presented in Sec. 4. We summarize the work in Sec. 5.

2. Theory

Suppose a Gaussian beam with a waist w_0 is incident on an objective lens with a high NA and an entrance pupil radius of R . We can think of three different regimes, namely, (i) $w_0 \ll R$, (ii) $w_0 \approx R$, and (iii) $w_0 \gg R$. We first consider a general theory which can address all three regimes and then discuss regimes (i) and (iii) as limiting cases of the general theory.

2.A. Field distribution near the focal region in general cases

We use the electromagnetic diffraction theory of Richards and Wolf,¹⁽³⁾ for the numerical calculation of the intensity distribution of the focused beam. For the integral, we choose our Cartesian coordinate system in the following way (see Fig. 1). The origin is located at the focus, z axis coincides with the optic axis of the optical system under consideration, pointing in the beam propagation direction and x axis points in the polarization direction of the

incident field e_0 . A time-independent part $e(r)$ of the analytical solution of the Helmholtz's equation for the electric field at a point $P(r)$ in the image space of our optical system is given by¹

$$e(r) = \frac{ikf}{2} \int \int \frac{a(s_x; s_y)}{s_z} e^{ikf(s_x; s_y) + s \cdot rg} ds_x ds_y; \quad (1)$$

where $s = (s_x; s_y; s_z)$ is a unit vector pointing in the direction of a ray, $(s_x; s_y)$ represents aberration in the optical system, Ω is the solid angle subtended by the exit pupil of the objective lens from the origin, the focus, and a , called an electric strength factor, is the electric field incident on the exit pupil after passing through the lens. Similarly, the magnetic field $h(r)$ can be written in the same way in terms of a different strength factor $b (= s \cdot a)$. Eq.(1) is valid only if $kf \gg \pi/4$, where f is focal length.

We introduce spherical polar coordinates $(\theta; \phi; \phi')$ for the point Q on the exit pupil and $(r; \theta; \phi)$ for the observation point P in the image space. The Cartesian components of the strength vector a can then be written as

$$a_x = e_0(\theta) \int \cos \theta [\cos \theta + \sin^2 \theta' (1 - \cos \theta)]; \quad (2a)$$

$$a_y = e_0(\theta) \int \cos \theta (\cos \theta - 1) \cos \theta' \sin \theta'; \quad (2b)$$

$$a_z = e_0(\theta) \int \cos \theta \sin \theta \cos \theta'; \quad (2c)$$

where $e_0(\theta)$ is the amplitude of the incident electric field e_0 . Similar expressions hold for the components of the magnetic field strength factor b . On substitution of Eq.(2) into Eq.(1) with $s = (\sin \theta \cos \theta'; \sin \theta \sin \theta'; \cos \theta)$, we obtain the following expressions for the Cartesian components of e .

$$e_x(r) = \frac{i}{2} kf (I_0 + I_2 \cos 2\theta); \quad (3a)$$

$$e_y(r) = \frac{i}{2} kf I_2 \sin 2\theta; \quad (3b)$$

$$e_z(r) = ikf I_1 \cos \theta; \quad (3c)$$

where

$$I_0(r; \theta) = \int_0^Z \frac{P}{e_0(\theta)} \cos\theta \sin\theta (1 + \cos\theta) J_0(kr \sin\theta \sin\theta) e^{ikr \cos\theta \cos\theta} d\theta; \quad (4a)$$

$$I_1(r; \theta) = \int_0^Z \frac{P}{e_0(\theta)} \cos\theta \sin^2\theta J_1(kr \sin\theta \sin\theta) e^{ikr \cos\theta \cos\theta} d\theta; \quad (4b)$$

$$I_2(r; \theta) = \int_0^Z \frac{P}{e_0(\theta)} \cos\theta \sin\theta (1 - \cos\theta) J_2(kr \sin\theta \sin\theta) e^{ikr \cos\theta \cos\theta} d\theta; \quad (4c)$$

where θ is a semi-aperture angle satisfying $\theta = 2(1 - \cos\theta)$ and its Sine value is the numerical aperture ($NA = \sin\theta$).

For a well-collimated Gaussian beam with a beam waist w_0 and an amplitude A_0 , $e_0(\theta)$ can be written as

$$e_0(\theta) = A_0 \exp[-(f \sin\theta/w_0)^2]; \quad (5)$$

under the Abbe's sine condition.¹⁰ The intensity distribution near the focus is then given by the time-averaged z-component of the Poynting vector:

$$S_z(r) = \frac{c(kf)^2}{32} f J_0^2 J_1^2 J_2^2; \quad (6)$$

where c denotes the speed of light in vacuum.

2.B. Large beam waist limit, $w_0 \gg R$

Since $w_0 \gg R$, we can approximate the incident Gaussian beam as a plane wave and use the results in the previous section with a substitution $e_0(\theta) = \text{const.}$ in Eq. (4).

i) Transverse spot size (x_{FWHM}).

The field distribution in the focal plane of the objective lens can be written as

$$\begin{aligned} I_0(r; \theta = \pi/2) &= \int_0^Z \frac{P}{e_0(\theta)} \cos\theta \sin\theta (1 + \cos\theta) J_0(kr \sin\theta) d\theta; \\ I_1(r; \theta = \pi/2) &= \int_0^Z \frac{P}{e_0(\theta)} \cos\theta \sin^2\theta J_1(kr \sin\theta) d\theta; \\ I_2(r; \theta = \pi/2) &= \int_0^Z \frac{P}{e_0(\theta)} \cos\theta \sin\theta (1 - \cos\theta) J_2(kr \sin\theta) d\theta; \end{aligned} \quad (7)$$

In general, $I_0 \approx I_1; I_2$ and thus the transverse spot size at focus is mostly determined by I_0 integral. Further approximation is then obtained by noting that the functional factor $(1 + \cos\#) = 2$ is approximately equal to $\frac{1}{\cos\#}$, which can be easily verified by Taylor series expansion of these two. This approximation is reasonably good even when $\# \neq 1$. For example, the difference between these two functional factors is 4.8% for $\# = 1$. Under this approximation, Eq. (7) becomes

$$I_0 = \frac{2}{\pi} \int_0^Z \cos\# \sin\# J_0(kr \sin\#) d\# / \frac{J_1(kr \sin\#)}{kr \sin\#}; \quad (8)$$

which is of the same form as the Fraunhofer diffraction by a circular aperture. Although the paraxial assumption $\sin\# \approx 1$ is used in the Fraunhofer diffraction theory, our approximate result, Eq. (8), is still applicable to non-paraxial cases with $\#$ up to the order of unity. The transverse spot size is then obtained from Eq. (8) as

$$x_{FWHM} \approx \frac{2}{k \sin\#} \frac{1.6163}{NA} = 0.5145 \frac{1}{NA} \quad (9)$$

Figure 2 shows the difference between x_{FWHM} approximated by Eq. (9) and the exact one by Eqs. (4) and (6). The approximation is excellent in that the difference is as small as 2.8% even when $NA = 1$, the largest possible NA value.

ii) Longitudinal spot size (z_{FWHM}).

The field distribution in the z -axis near the focus is given by

$$I_0(r; z=0) = \frac{2}{\pi} \int_0^Z \cos\# \sin\# (1 + \cos\#) e^{ikz \cos\#} d\#; \\ I_1(r; z=0) = I_2(r; z=0) = 0; \quad (10)$$

Under the same approximation as above,

$$I_0 = \frac{2}{\pi} \int_0^Z \cos\# \sin\# e^{ikz \cos\#} d\# \\ = \frac{2}{(kz)^2} \int_0^Z \frac{1}{\cos\#} e^{iq} dq \\ / \sin^2 \frac{x}{2} \frac{\sin x}{x} - i \tan^2 \frac{x}{2} \frac{x \cos x}{x^2} \frac{\sin x}{x^2} \quad (11)$$

where $x = kz \sin\# (\approx 2)$. For $\#$ up to unity, the contribution from the second term in $\int I_0^2$ is negligibly small, proportional to $\tan^4 \frac{x}{2} < 0.089$, and thus $\int I_0^2$ is approximately given by

the Sinc function squared, which is the same as the Fraunhofer diffraction result except that x is proportional to $\sin^2(\frac{\theta}{2})$ not to $\sin^2(\theta)$ in the usual Fraunhofer diffraction. For an arbitrary θ , z_{FWHM} is obtained from Eq. (11) as

$$z_{FWHM} = \frac{(\quad)}{4 \sin^2 \frac{\theta}{2}} = \frac{(\arcsin NA)}{4 \sin^2 (\frac{1}{2} \arcsin NA)} \quad (12)$$

where the slowly varying function (\quad) is plotted in Fig. 3. For θ up to unity, we can approximate $(\quad)' \approx (0)' \approx 1.772$, by which our error is only 1.7% for $\theta = 1$ and 5.4% for $\theta = 1.25$, which corresponds to $NA = 0.95$. Under this approximation,

$$z_{FWHM} \approx \frac{1.772}{4 \sin^2 \frac{\theta}{2}} = \frac{1.772}{4 \sin^2 (\frac{1}{2} \arcsin NA)} \quad (13)$$

which reduces to the usual Fraunhofer diffraction result

$$z_{FWHM} \approx \frac{1.772}{\theta^2} \approx \frac{1.772}{NA^2}; \quad (14)$$

under the paraxial condition, $\theta \ll 1$.

2.C. Small beam waist limit, $w_0 \ll R$

Although the numerical aperture of the lens is assumed to be large, only the central portion of the objective lens is utilized by the incident Gaussian beam when $w_0 \ll R$. One can define an effective numerical aperture NA_e as $NA_e = w_0/f \ll 1$, and thus the paraxial approximation can be effectively applied. One is allowed to use Gaussian optics to calculate the beam size in the focal region. Particularly, when the incident beam has a minimum waist at the entrance pupil of the objective lens, the Gaussian optics provides a simple formula for the field distribution in the region of focus.

i) Transverse spot size (x_{FWHM}).

The Gaussian beam waist w_0^0 in the region of focus is given by

$$w_0^0 = \frac{f}{w_0} \quad (15)$$

where w_0 is the minimum beam waist of the incident beam located at the entrance pupil of the objective lens. The above 1/e-width can be converted to a full width at half maximum as

$$x_{FWHM} = 2 \sqrt{\ln 2} \frac{f}{w_0} \approx 0.375 \frac{f}{NA_e}; \quad (16)$$

where $NA_e = w_0/f$.

We can also derive the above result from the I integrals for general cases. From Eq. (4), the field distribution in the focal plane can be written as

$$\begin{aligned}
 I_0(r; z=2) &= \int_0^Z e_0(\theta) \cos\theta \sin\theta (1 + \cos\theta) \\
 &\quad J_0(kr \sin\theta) d\theta; \\
 I_1(r; z=2) &= \int_0^Z e_0(\theta) \cos\theta \sin^2\theta \\
 &\quad J_1(kr \sin\theta) d\theta; \\
 I_2(r; z=2) &= \int_0^Z e_0(\theta) \cos\theta \sin\theta (1 - \cos\theta) \\
 &\quad J_2(kr \sin\theta) d\theta;
 \end{aligned} \tag{17}$$

where $e_0(\theta)$ is given by Eq. (5). Since $e_0(\theta)$ is significant only when $\sin\theta \approx w_0/f \approx 1$, the integrands above count only when $\theta \approx 1$, and thus we can rewrite the above as

$$\begin{aligned}
 I_0 &\approx \int_0^Z e_0(\theta) \theta J_0(kr\theta) d\theta; \\
 I_1 &\approx \int_0^Z e_0(\theta) \theta^2 J_1(kr\theta) d\theta; \\
 I_2 &\approx \frac{1}{2} \int_0^Z e_0(\theta) \theta^3 J_2(kr\theta) d\theta;
 \end{aligned} \tag{18}$$

Since $I_1 \approx I_0 (w_0/f)^2 \approx 1$ and $I_2 \approx I_0 (w_0/f)^4 \approx 1$, the field distribution is mostly determined by I_0 . We can further simplify the I_0 integral as

$$\begin{aligned}
 I_0 &\approx \int_0^Z e^{-\frac{f\theta}{w_0}} \theta J_0(kr\theta) d\theta \\
 &\approx \int_{f/w_0}^0 e^{x^2} x J_0\left(\frac{krw_0}{f}x\right) dx \\
 &= \int_0^1 e^{x^2} x J_0(x) dx = e^{(-2)} \approx 0.135
 \end{aligned} \tag{19}$$

where $x = krw_0/f$, from which we obtain an 1-e width of the field distribution as $2f = kw_0$, which is nothing but w_0^0 in Eq. (15).

ii) Longitudinal spot size (z_{FWHM}).

In Gaussian optics, the Rayleigh range z_0^0 in the region of focus is given by

$$z_0^0 = \frac{w_0^2}{4\lambda} = -\frac{f}{w_0} \tag{20}$$

The FWHM value in the z direction is just twice of the Rayleigh range.

$$z_{FWHM} = 2z_0^0 = -\frac{2f}{w_0}, \quad 0.6366 \frac{f}{NA_e^2} \tag{21}$$

We can also derive Eq. (21) from Eq. (4):

$$\begin{aligned}
I_0(r; = 0) &= \int_0^Z e_0(\#) \cos\# \sin\# (1 + \cos\#) e^{ikr \cos\#} d\#; \\
I_1(r; = 0) &= 0 = I_2(r; = 0):
\end{aligned} \tag{22}$$

Again, the integrand is significant only when $\# \approx w_0 = f^{-1}$, and thus

$$\begin{aligned}
I_0 &/ \int_0^Z e^{x^2} x e^{ikr [1 - \frac{1}{2}(w_0 x = f)^2]} dx \\
&= \frac{1}{2} e^{ikr} \int_0^Z e^q e^{\frac{i}{2}kr(w_0 = f)^2 q} dq \\
&/ \left(1 + i \frac{krw_0^2}{2f^2} \right)^{-1};
\end{aligned} \tag{23}$$

and thus the intensity distribution is proportional to a Lorentzian

$$I_0^2 / \frac{1}{r^2 + \frac{2f^2}{kw_0^2}}; \tag{24}$$

from which we obtain $z_{FWHM} = 4f^2 = kw_0^2$ identical to the one in Eq. (21).

2.D . Application to NA= 0.4, 0.75 and 0.95

In Fig. 4, theoretical x_{FWHM} and z_{FWHM} values for NA= 0.4, 0.75, 0.95, respectively, are plotted. The solid lines represent FWHM's calculated from Eqs. (4) and (6). The dash-dotted lines in Figs. 4 (a), (c) and (e) are calculations based on Eqs. (16) and those in Figs. 4 (b), (d) and (f) are given by Eq. (21). Similarly, the dashed lines are calculated from Eqs. (9) and (13). These dash-dotted and dashed lines represent two limiting cases, $w_0 = R^{-1}$ and $w_0 = R^{-1}$, respectively, of the general curves which are valid for any $w_0 = R$ values for given NA's.

3. Experimental Setup

Our experimental setup is shown in Fig. 5. A He-Ne laser (Uniphase, 4mW, 632.8nm) with x-polarization was first incident on a spatial filter, and then expanded and collimated to a Gaussian beam with a beam waist w_0 and its profile was measured on a CCD. An objective lens was mounted on a xyz-translation stage with its z coordinate scanned by a PZT stack so that it could be coarse-positioned manually and fine-scanned by the PZT in the z direction. An infinity-corrected microscope objective lens with NA= 0.4, 0.75 (both from NIKON) and 0.95 (from OLYMPUS) were used. A pinhole (National Aperture, $\phi = 0.5 \pm 0.1$ mm), which served as an intensity probe, was mounted on a translation stage with PZT stacks for

scanning in the x- and y directions. The thickness of the pinhole substrate (stainless steel) was about 10 μm , and thus the opening was in a shape of a cylinder. The diameter of the opening was about 1 μm near the surface of the substrate, but it decreased to 0.5 μm near the center of the substrate. The light transmitted through the pinhole was detected by a photomultiplier tube and the signal was digitized by a data acquisition board on a computer as a function of x- and y-PZT control voltages. A resulting image amounted to a 400 \times 300 array.

4. Results and Discussions

We measured the intensity distribution for a Gaussian beam with an initial beam waist of $w_0 = 0.46, 1.02, 1.48, 2.48, 3.37$, and 5.61 mm . From the measured intensity distribution in the xy focal plane, we determined the full width at half maximum (FWHM) in the x direction (x_{FWHM}), and similarly from that in the yz meridional plane, we measured the FWHM in the z direction (z_{FWHM}). For instance, the intensity profile created by an objective lens with $\text{NA} = 0.95$ for an input beam of $w_0 = 5.61 \text{ mm}$ is shown in Fig. 6. Since the entrance pupil radius R of the objective lens was 1.71 mm , the incident beam could be considered a plane wave. The xy profiles in Fig. 6 were measured at an interval of 0.2 mm in the z direction. The direction of beam propagation was from frame 1 to frame 12 in Fig. 6. The xy- and yz profiles corresponded to an actual area of $4.64 \text{ mm} \times 3.48 \text{ mm}$ and $4.64 \text{ mm} \times 3.00 \text{ mm}$, respectively. The measured x- and z-FWHM values were 0.49 mm and 0.9 mm , respectively.

The time-averaged z component of the Poynting vector in the near focus was calculated from Eq. (6). To compare experiment with theory, we assumed that the total amount of light detected by the PMT through the pinhole was proportional to the convolution of the z component of the Poynting vector with the pinhole opening.

$$S_z(x; y) = \int_{-\infty}^{\infty} \int_{-\infty}^{\infty} S_z(x^0; y^0) P(x - x^0; y - y^0) dx^0 dy^0 \quad (25)$$

where $P(x; y)$ is an aperture function for the pinhole. This assumption is equivalent to saying that the possible field distortion by the conducting surface of the pinhole substrate does not affect the amount of energy flow through the pinhole much so that we just integrate the normal component of the unperturbed Poynting vector calculated for the absence of the pinhole over the aperture function of the pinhole. The validity of this assumption is justified below.

The dependence of the measured x- and z-FWHM values on the input Gaussian waist w_0 for $\text{NA} = 0.4, 0.75$ and 0.95 are shown in the Fig. 7, where (a) and (b) are for $\text{NA} = 0.4$, (c) and (d) for $\text{NA} = 0.75$ and (e) and (f) for $\text{NA} = 0.95$, respectively. FWHM values obtained from convoluted $S_z(x; y)$ are represented by solid lines and experimental results are drawn by square dots. The agreement between experiment and theory is reasonably good. Particularly,

the agreement is quite good for both large ($w_0 \gg R$) and small ($w_0 \ll R$) beam waists. Discrepancies are relatively large for intermediate beam waists ($w_0 \sim R$).

When w_0 is equal to the radius of the entrance pupil R , which was 4.0, 3.0, 1.72 mm for $NA = 0.4, 0.75, 0.95$, respectively, the resulting theoretical FWHM values differ by less than 5% from those ultimate FWHM values, which occur when $w_0 \ll R$, as can be seen in Fig. 4 whereas the experimental FWHM values differ by at most 20% (see Fig. 7) from the convoluted ultimate FWHM's. When w_0 is reduced to $R/2$, the increase in theoretical FWHM values are much less than twice, being about 20% for $NA = 0.4$ and 0.75 and about 80% for $NA = 0.95$. The increase in measured FWHM values are more than in those theoretical ones, being about 100% for all except for the z-FWHM values for $NA = 0.4$. The smallest measured x- and z-FWHM values are (0.99 μm , 6.05 μm) for $NA = 0.4$, (0.59 μm , 1.55 μm) for $NA = 0.75$ and (0.49 μm , 0.9 μm) for $NA = 0.95$. These values were reasonably well matched with the convoluted FWHM values.

The discrepancies between theory and experiment including the large ones for $NA = 0.4$ may come from two possible causes. One is the field distortion caused by the pinhole itself. This effect should be less serious for large beam waists than the small beam waists. However, the discrepancies were mostly observed for large beam waists as in the case of $NA = 0.4$, and thus the field-distortion does not appear to be the major source of the observed discrepancies. The more possible source of discrepancy is the aberration of the microscope objective lens itself. The fact that the discrepancies were more serious in z-FWHM values than in x-FWHM values support this reasoning.

5. Summary and Conclusion

We studied the intensity distribution in the region of focus when a linearly-polarized well collimated Gaussian beam with a waist of w_0 was incident on a high-NA objective lens with an entrance pupil radius of R . We first theoretically examined the transverse spot size x_{FWHM} and the longitudinal spot size z_{FWHM} near the focal plane for an arbitrary input beam waist w_0 . We used the vectorial diffraction theory of Richards and Wolf and calculated a time-averaged Poynting vector in the near focus. We then derived approximate expressions for FWHM's for two limiting cases, $w_0 \gg R$ and $w_0 \ll R$. Surprisingly, we found that the Fraunhofer diffraction results can well approximate correct FWHM's for NA up to $\sin(1) \approx 0.84$.

In experiments, we varied the initial w_0 for a given NA 's of 0.4, 0.75 and 0.95 and measured x_{FWHM} and z_{FWHM} values. They were obtained by scanning a pinhole of 0.5 μm diameter across the focused beam and by measuring the total transmitted light through the pinhole. The results obtained by convoluting the calculated Poynting vector with the pinhole were well matched with the measured intensity distributions. The smallest measured x- and z-FWHM

values were $0.49 \mu\text{m}$ and $0.9 \mu\text{m}$, respectively, for $\text{NA} = 0.95$ with $\lambda = 632.8 \text{ nm}$.

We found that when $w_0 = R$ both x- and z-FWHM values differ by less than 5% from their ultimate FWHM values in our calculations and by at most 20% even in actual measurements. We also found that one can allow the initial beam waist as small as $R=2$ only to increase the FWHM values by twice from the ultimate FWHM values.

Acknowledgments

This work was supported by Korea Research Foundation Grant (KRF-2002-070-C00044).

References

1. E. Wolf, "Electromagnetic Diffraction in Optical Systems - An Integral Representation of the Image Field", *Proc. Roy. Soc. A* 253, 349 (1959).
2. B. Richards and E. Wolf, "Electromagnetic Diffraction in Optical Systems - Structure of the Image Field in an Aplanatic System", *Proc. R. Soc. A* 253, 358 (1959).
3. M. Mansuripur, "Certain computational aspects of vector diffraction problems", *J. Opt. Soc. Am. A* 6, 786 (1989).
4. M. Born and E. Wolf, *Principles of optics*, 7th (expanded) Ed. (Cambridge University Press, Cambridge, 1999).
5. J. J. Stamnes, *Waves in Focal Regions* (Adam Hilger, Bristol and Boston, 1986).
6. S. Quabis, R. Dorn, M. Eberler, O. Glockl and G. Leuchs, "The Focus of light - theoretical calculation and experimental tomographic reconstruction", *Appl. Phys. B* 72, 109 (2001).
7. R. Dorn, S. Quabis and G. Leuchs, "The focus of light-linear polarization breaks the rotational symmetry of the focal spot", *J. Mod. Opt.* 50, 1917 (2003).
8. S. K. Rhodes, A. Barty, A. Roberts and K. A. Nugent, "Sub-wavelength characterization of optical focal structures", *Opt. Commun.* 145, 9 (1989).
9. S. K. Rhodes, K. A. Nugent and A. Roberts, "Precision measurement of the electromagnetic fields in the focal region of a high-numerical-aperture lens using a tapered fiber probe", *J. Opt. Soc. Am. A* 19, 1689 (2002).
10. M. Mansuripur, *Classical Optics and its Applications* (Cambridge University Press, Cambridge, 2002).

List of Figure Captions

Fig. 1. Coordinate system for the calculation of the intensity distribution in the region of focus

Fig. 2. Error in x_{FWHM} approximated by Eq. (9) with respect to the exact one by Eqs. (4) and (6) as a function of NA.

Fig. 3. Numerical factor (\cdot) in Eq. (12).

Fig. 4. Dependence of transverse and longitudinal FWHM values, x_{FWHM} and z_{FWHM} , respectively, on w_0 of the incident Gaussian beam. Vertical dotted lines indicate $w_0 = R=2;R$. (a)–(b) NA = 0.4, (c)–(d) NA = 0.75, and (e)–(f) NA = 0.95.

Fig. 5. Experimental setup for measuring the profile of the beam focused by an objective lens. L1, L2, L3: lenses, BS: beam splitter, TS1, TS2: translation stages with PZT actuators, OL: objective lens, CCD: charge-coupled device detector, P1, P2: pinholes, C: condenser, PMT: photomultiplier tube, and A1, A2, A3: PZT control voltage signals from an analog-digital converter board on a personal computer. A1 controls the z translation of the objective lens and A2 and A3 control the x, and y translation of the pinhole stage. L1, P1, and L2 form a spatial filter.

Fig. 6. Transverse (xy) and longitudinal (yz) profiles in the near focus for NA = 0.95 objective lens. Scan areas for xy- and yz profiles were $4.64 \text{ m} \times 3.48 \text{ m}$ and $4.64 \text{ m} \times 3.00 \text{ m}$, respectively.

Fig. 7. Dependence of transverse (x) and longitudinal (z) FWHM values on w_0 of the incident Gaussian beam. The FWHM values obtained from Eq. (25) were represented by solid lines and experimental results were drawn by square dots. Vertical dotted lines indicate $w_0 = R=2;R$. (a)–(b): NA = 0.4, (c)–(d): NA = 0.75, and (e)–(f): NA = 0.95.

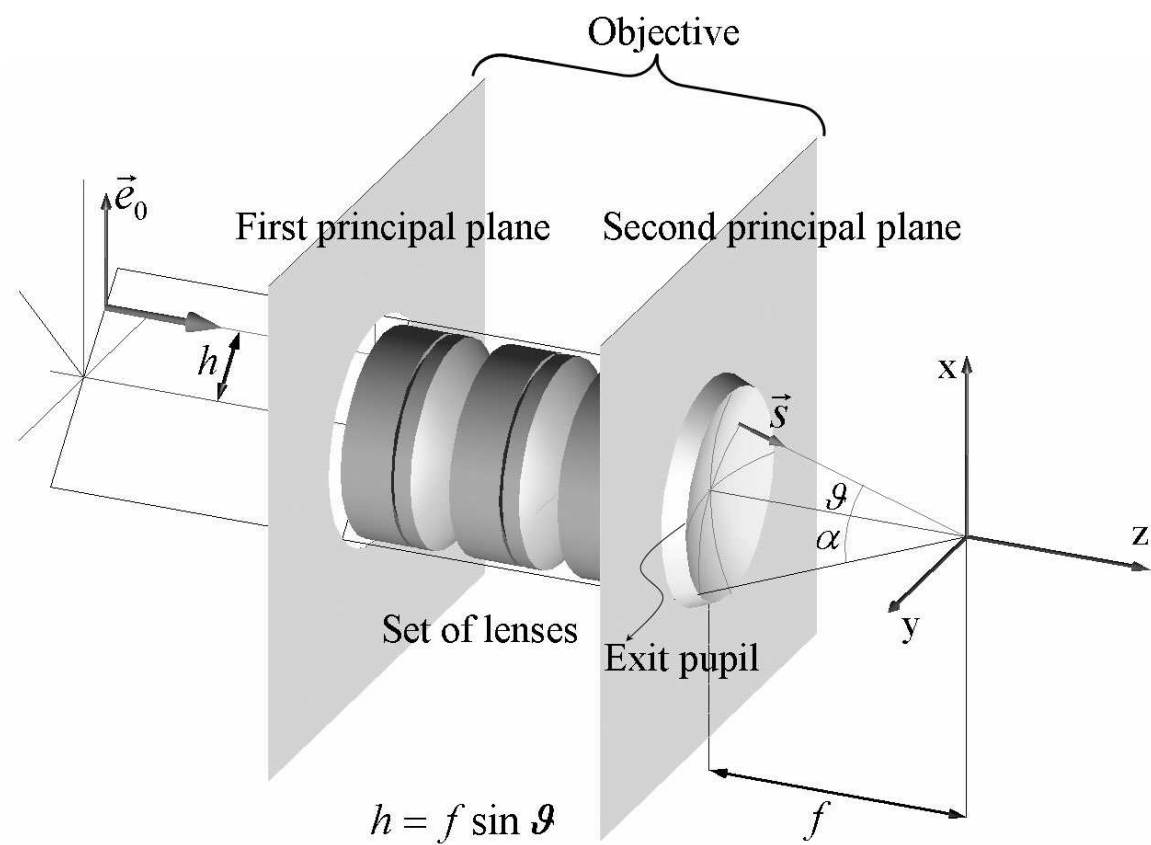


Fig. 1.

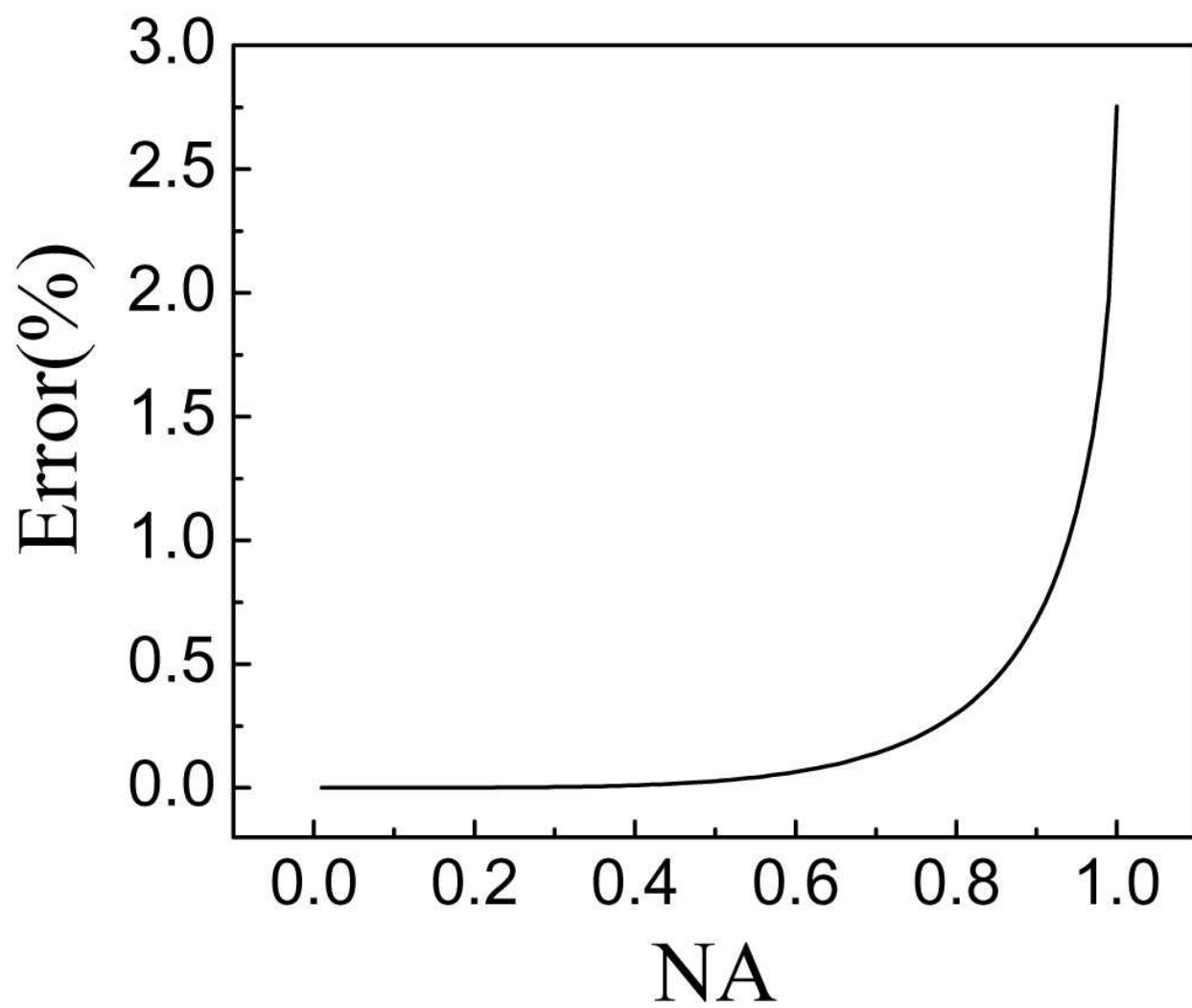


Fig. 2.

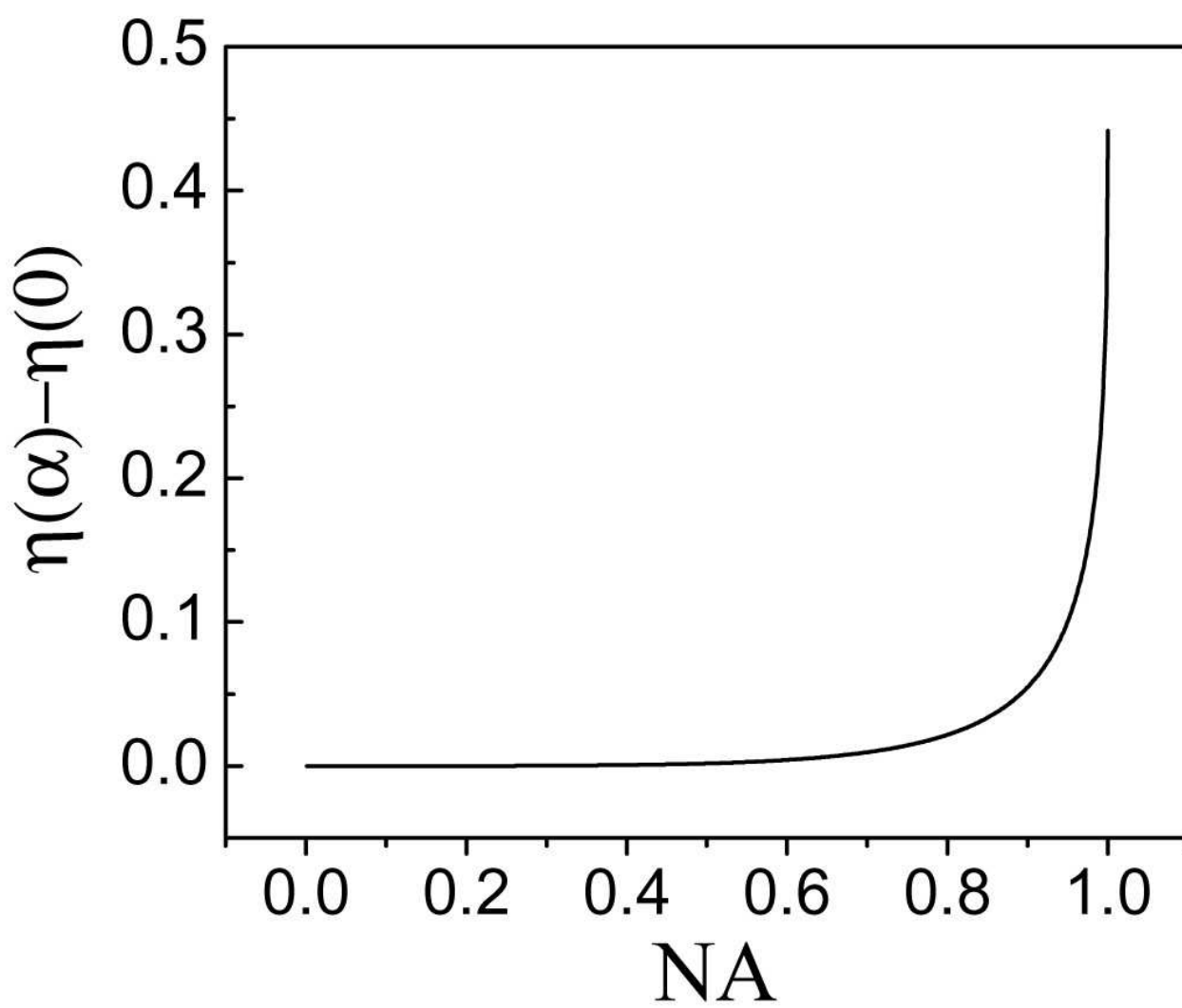
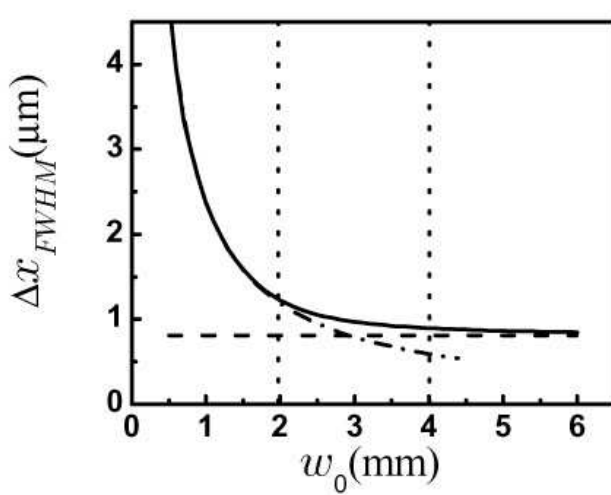
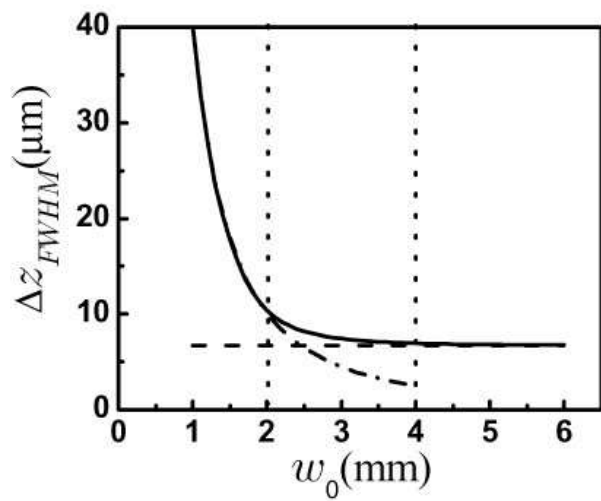


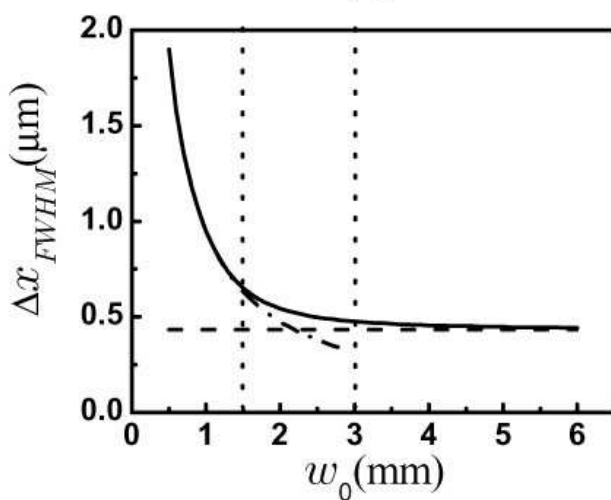
Fig. 3.



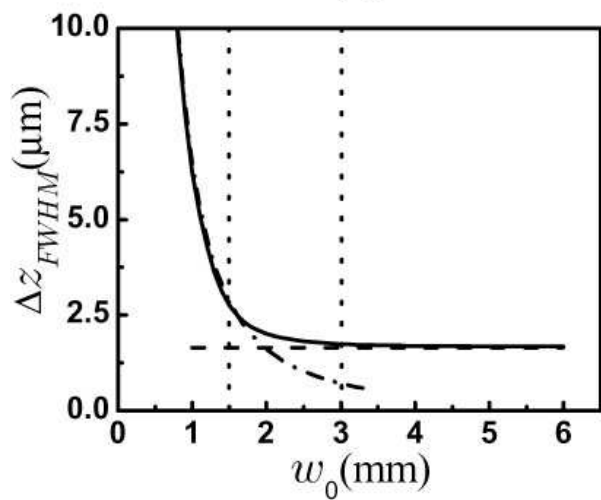
(a)



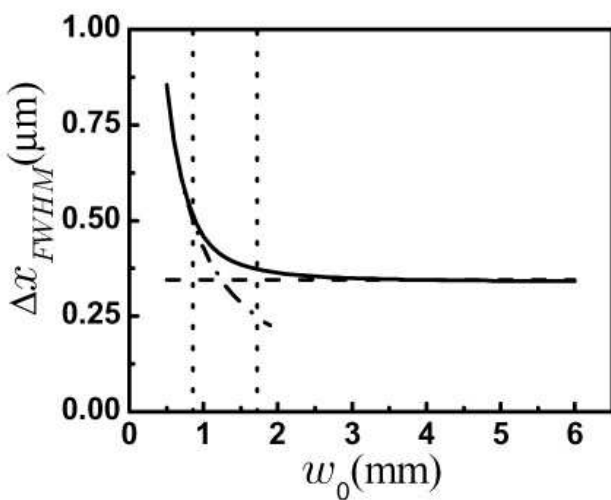
(b)



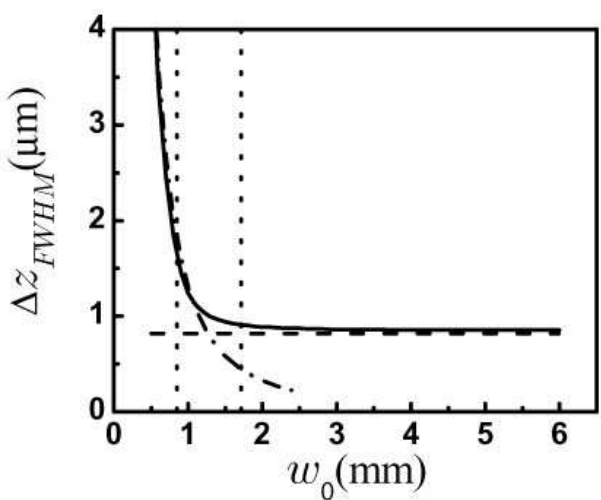
(c)



(d)



(e)



(f)

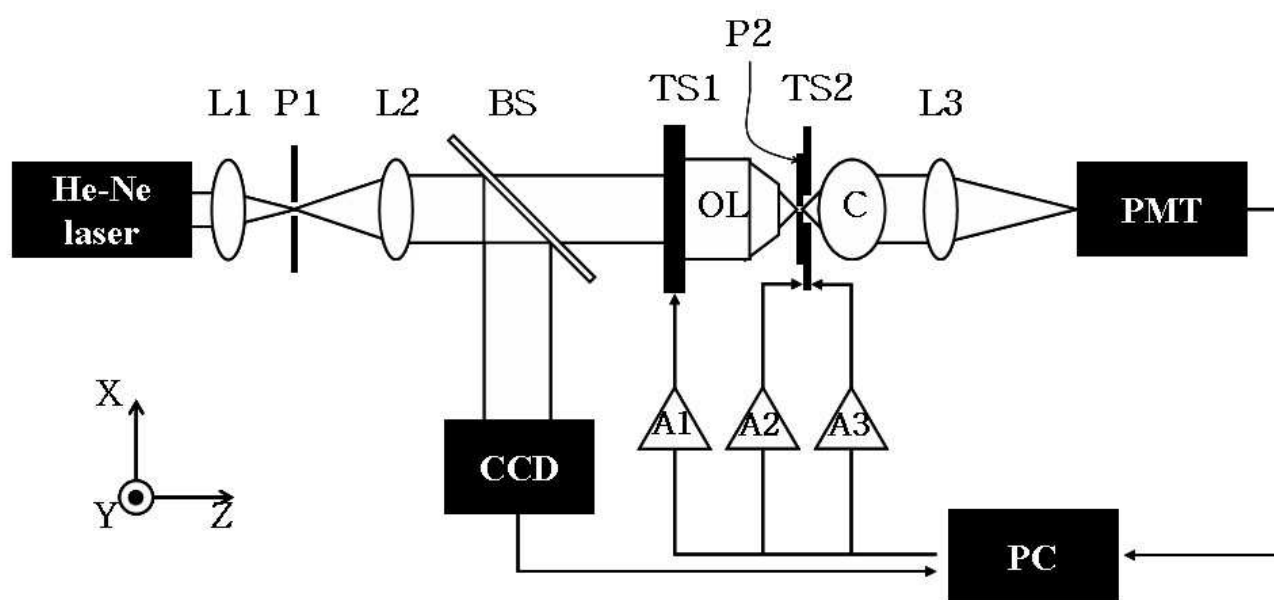


Fig. 5.,

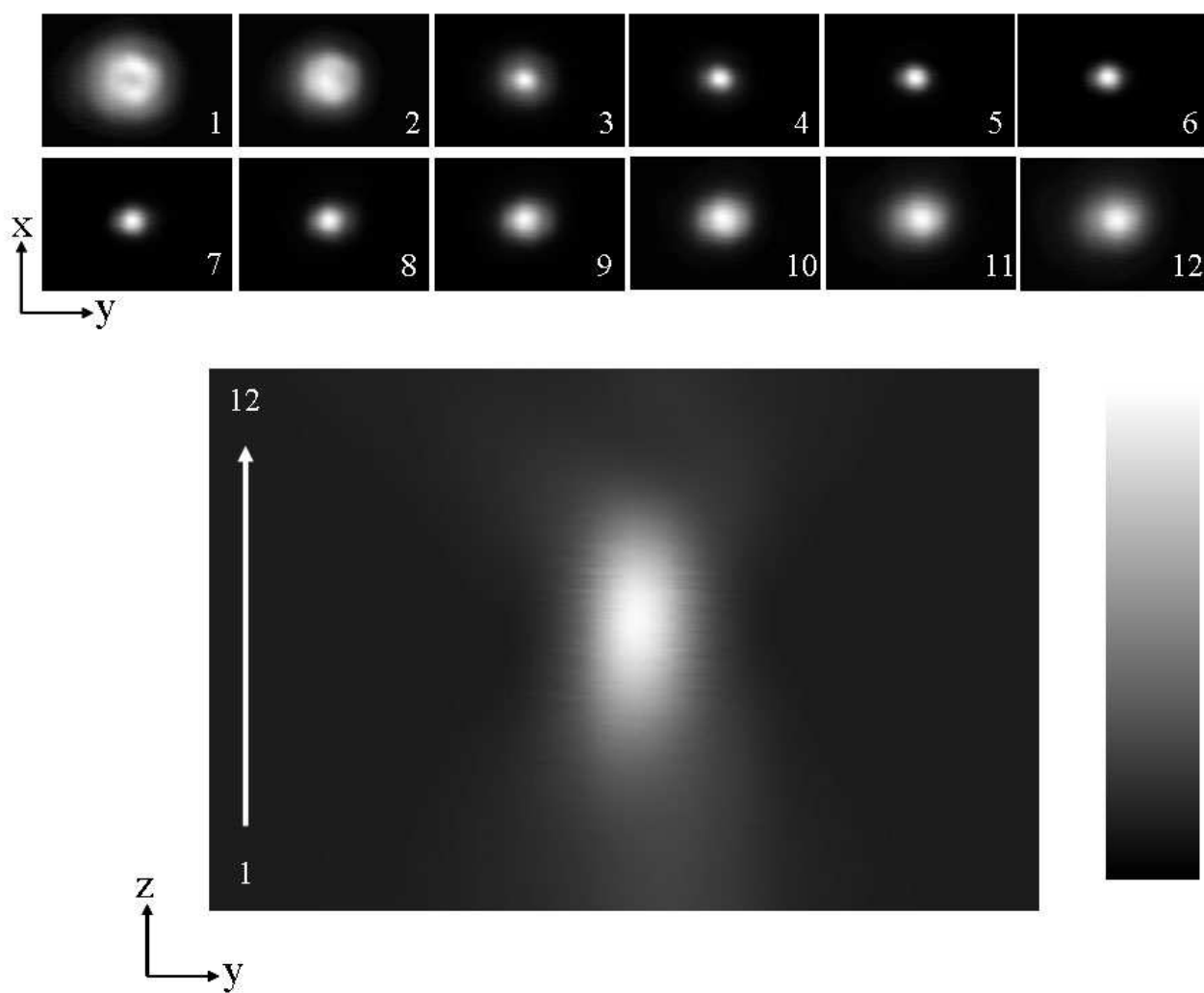
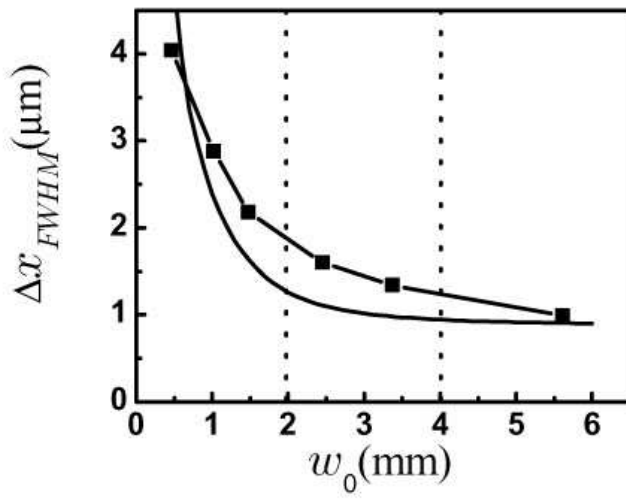
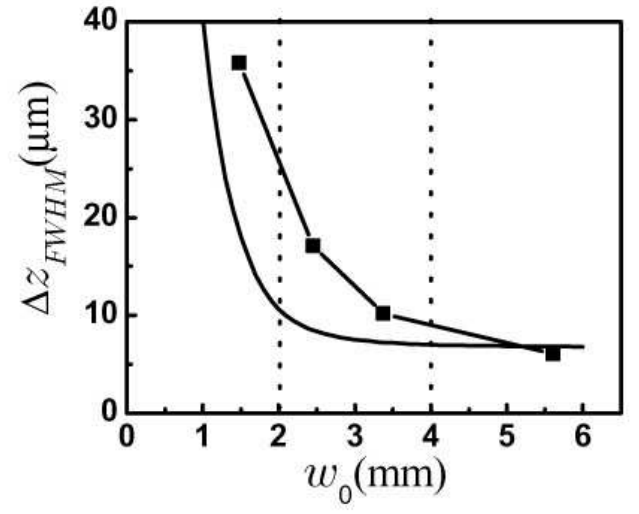


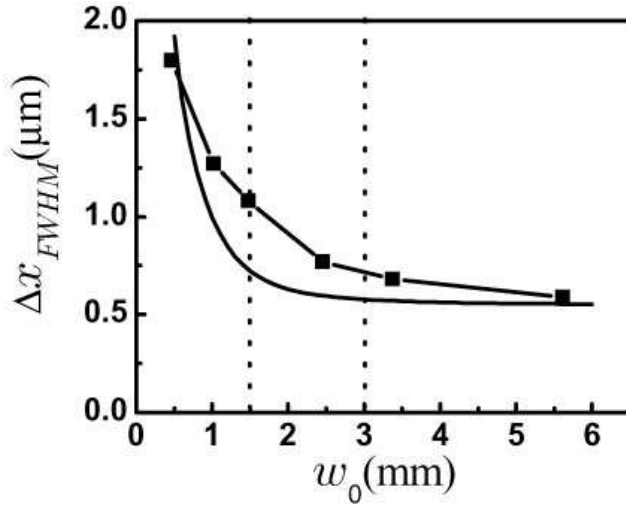
Fig. 6.



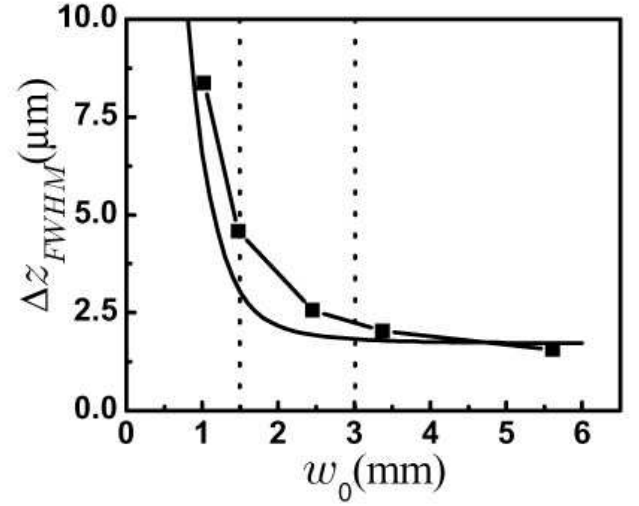
(a)



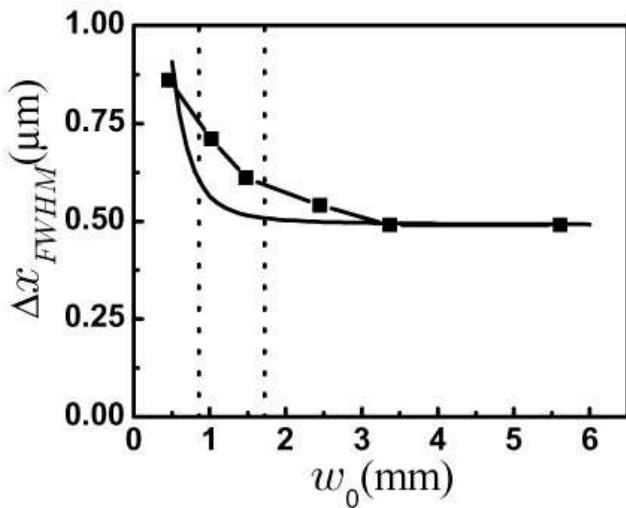
(b)



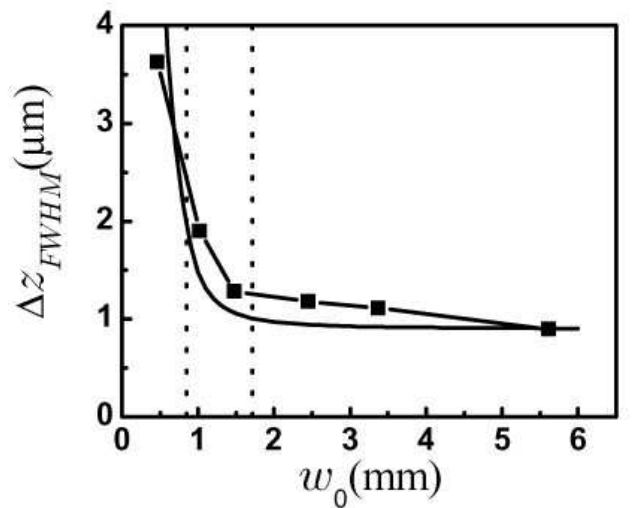
(c)



(d)



(e)



(f)